# COSMIC GALAXY-IGM HI RELATION AT $z\sim 2-3$ PROBED IN THE COSMOS/ULTRAVISTA 1.6 DEG<sup>2</sup> FIELD

Shiro Mukae<sup>1,2</sup>, Masami Ouchi<sup>1,3</sup>, Koki Kakiichi<sup>4</sup>, Nao Suzuki<sup>3</sup>, Yoshiaki Ono<sup>1</sup>, Zheng Cai<sup>5</sup>, Akio K. Inoue<sup>6</sup>, Yi-Kuan Chiang<sup>7</sup>, Takatoshi Shibuya<sup>1</sup>, Yuichi Matsuda<sup>8,9</sup> Submitted to ApJ

#### ABSTRACT

We present spatial correlations of galaxies and IGM neutral hydrogen H<sub>I</sub> in the COSMOS/UltraVISTA 1.62 deg<sup>2</sup> field. Our data consist of 13,415 photo-z galaxies at  $z \sim 2-3$  with  $K_s < 23.4$  and the Ly $\alpha$ forest absorptions in the background quasar spectra selected from SDSS data with no signature of damped Ly $\alpha$  system contamination. We estimate a galaxy overdensity  $\delta_{\rm gal}$  in an impact parameter of 2.5 (proper) Mpc, and calculate the Ly $\alpha$  forest fluctuations  $\delta_{\langle F \rangle}$  whose negative values correspond to the strong Ly $\alpha$  forest absorptions. We identify a weak anti-correlation between  $\delta_{\rm gal}$  and  $\delta_{\langle F \rangle}$  with a Spearman's rank correlation coefficient of -0.39 suggesting that the galaxy overdensities and the Ly $\alpha$ forest absorptions positively correlate in space at the  $\sim 90\%$  confidence level. This positive correlation indicates that high-z galaxies exist around an excess of HI gas in the Ly $\alpha$  forest. We find four cosmic volumes, dubbed  $A_{\rm obs}$ - $D_{\rm obs}$ , that have extremely large (small) values of  $\delta_{\rm gal} \simeq 0.8$  (-1) and  $\delta_{\langle F \rangle}$  $\simeq 0.1$  (-0.4), three out of which, B<sub>obs</sub>-D<sub>obs</sub>, significantly depart from the  $\delta_{\rm gal}$ - $\delta_{\langle F \rangle}$  correlation, and weaken the correlation signal. We perform cosmological hydrodynamical simulations, and compare with our observational results. Our simulations reproduce the  $\delta_{\rm gal}$ - $\delta_{\langle F \rangle}$  correlation, agreeing with the observational results. Moreover, our simulations have model counterparts of A<sub>obs</sub>-D<sub>obs</sub> and suggest that the observations pinpoint, by chance, a galaxy overdensity like a proto-cluster, gas filaments lying on the quasar sightline, a large void, and orthogonal low-density filaments. Our simulations indicate that the significant departures of  $B_{obs}$ - $D_{obs}$  are produced by the filamentary large-scale structures and the observation sightline effects.

Keywords: intergalactic medium — quasars: absorption lines — large-scale structure of universe — galaxies: formation

### 1. INTRODUCTION

The link between baryons and the cosmic web is a clue to understand both the galaxy formation and the baryonic processes in the large-scale structures (LSSs). The processes between galaxies and the intergalactic medium (IGM) are the inflow which represents gas accretion on to galaxies and the outflow driven by supernovae and active galactic nuclei. Neutral hydrogen HI in the IGM is probed with the Ly $\alpha$  forest absorptions in spectra of background quasars (e.g., Faucher-Giguère et al. 2008; Becker et al. 2013; Prochaska et al. 2013) and bright star-forming galaxies (e.g., Steidel et al. 2010;

mukae@icrr.u-tokyo.ac.jp

<sup>1</sup> Institute for Cosmic Ray Research, The University of Tokyo, 5-1-5 Kashiwanoha, Kashiwa, Chiba 277-8582, Japan

<sup>2</sup> Department of Astronomy, Graduate School of Science, The University of Tokyo, 7-3-1 Hongo, Bunkyo, Tokyo, 113-0033, Japan

<sup>3</sup> Kavli Institute for the Physics and Mathematics of the Universe (Kavli IPMU, WPI), University of Tokyo, 5-1-5 Kashiwanoha, Kashiwa, Chiba, 277-8583, Japan

<sup>4</sup> Max Planck Institute for Astrophysics, Karl-Schwarzschild-Strasse 1, D-85748 Garching bei München, Germany

<sup>5</sup> UCO/Lick Observatory, University of California, 1156 High Street, Santa Cruz, CA 95064, USA

<sup>6</sup> College of General Education, Osaka Sangyo University, 3-1-1, Nakagaito, Daito, Osaka 574-8530, Japan

7 Department of Astronomy, University of Texas at Austin, 1 University Station C1400, Austin, TX 78712, USA

8 National Astronomical Observatory of Japan, Osawa 2-21-1, Mitaka, Tokyo 181-8588, Japan

<sup>9</sup> Graduate University for Advanced Studies (SOKENDAI), Osawa 2-21-1, Mitaka, Tokyo 181-8588, Japan

Thomas et al. 2014; Mawatari et al. 2016). The detailed properties of galaxy-IGM H<sub>I</sub> relations (hereafter galaxy-HI relation) have been studied by spectroscopic observations of the Keck Baryonic Structure Survey (KBSS: Rudie et al. 2012; Rakic et al. 2012; Turner et al. 2014) and other programs (Adelberger et al. 2003, 2005; Crighton et al. 2011). These spectroscopic observations target HI gas of the circumgalactic medium (CGM) around Lyman break galaxies (LBGs) that are high-z star-forming galaxies identified with a bright UV and blue continuum. These LBG spectroscopy for the galaxy-HI studies alone do not answer to the following two questions. One is the relation between IGM HI and galaxies that are not selected as LBGs. Because LBGs are identified in their dust-poor star-forming phase, dustrich and old-stellar population galaxies are missing in the past studies. In fact, the average star-formation duty cycle (DC) of LBGs is estimated to be  $\sim 30-60\%$ (Lee et al. 2009; Harikane et al. 2016). A large fraction of galaxies are not investigated in the studies of the galaxy-HI relation. The other question is what the galaxy-HI relation in a large-scale is. To date, the previous studies have investigated LBG-HI relations around sightlines of background quasars within  $\sim 30' \times 30'$ (c.f., Adelberger et al. 2003, 2005; Crighton et al. 2011; Rudie et al. 2012; Rakic et al. 2012; Turner et al. 2014). The galaxy-H<sub>I</sub> relation in a large-scale ( $\sim 1 \text{ deg}^2$ ) at high-z is not studied. Cai et al. (2015) have studied the galaxy-H<sub>I</sub> relation focusing on extremely massive overdensities with  $\sim 6,000$  SDSS quasar spectra by the MAp-

ping the Most Massive Overdensity Through Hydrogen (MAMMOTH) survey, but the galaxy-HI relations have not been systematically explored.

We investigate spatial correlations of  $K_s$ -band selected galaxies with no DC dependence and IGM HI at  $z \sim 2-3$  in a large 1.62 deg<sup>2</sup> area of COSMOS/UltraVISTA field, in conjunction with the comparisons with our models of the cosmological hydrodynamical simulations.

Our study of the galaxy-HI spatial correlation is complementary to the on-going programs of the MAMMOTH and the Ly $\alpha$  forest tomography survey of the COSMOS Lyman-Alpha Mapping And Tomography Observations (CLAMATO: Lee et al. 2014, 2016) which aims at illustrating the distribution of IGM HI gas in LSSs. In contrast, our study focuses on a spatial relation between galaxies and IGM HI gas.

This paper is organized as follows. We describe the details of our sample galaxies and background quasars in Section 2. In Section 3, our data analysis is presented. We investigate the galaxy-HI relation based on the observational data in Section 4. We introduce our simulations to examine the galaxy-HI relation of our observational results in Section 5. In Section 6, we compare observation and simulation results, and interpret our observational findings. Finally, we summarize our results in Section 7.

Throughout this paper, we adopt AB magnitudes (Oke & Gunn 1983). We use a cosmological parameter set of  $(\Omega_m, \Omega_\Lambda, \Omega_b, \sigma_8, n_s, h) = (0.26, 0.74, 0.045, 0.85, 0.95, 0.72)$  consistent with Planck2015 result (Planck Collaboration et al. 2015). We denote pkpc and pMpc (ckpc and cMpc) to indicate distances in proper (comoving) units.

#### 2. DATA

# 2.1. Photometric Galaxy Samples

We investigate galaxy overdensities in the COS-MOS/UltraVISTA field. Our photometric samples consist of the COSMOS/UltraVISTA catalog that is a  $K_s$ -band selected galaxy catalog (Muzzin et al. 2013a) covering the  $1.62 \, \deg^2$  area atop the UltaVISTA (McCracken et al. 2012) imaging data in the COSMOS field (Scoville et al. 2007). We use these photo-z galaxies at  $z \sim 2-3$ , following the selection criteria of Chiang et al. (2014) who have found galaxy overdensities in the COSMOS/UltraVISTA catalog. We apply a 90% completeness limit of  $K_s < 23.4$  mag that corresponds to a stellar mass limit of  $\log_{10}(M_*/M_\odot) > 9.7$ . This stellar mass limit is as large as  $\sim 0.1 M^*$  at  $z \sim 2.5$  where  $M^*$  is the characteristic stellar mass of a Schechter function parameter (Schechter 1976) for the stellar mass functions (SMFs) taken from Muzzin et al. (2013b). We remove objects ( $\sim 4\%$ ) whose photometric redshifts show broad and/or multi-modal redshift probability distributions indicating poorly determined redshifts. Here, the photo-zgalaxies that we use have the redshift distribution function whose 80%-tile probability distribution extend no larger than  $\Delta z = 0.2$  from the best estimate redshift. Finally, our photometric samples consist of 13,415 photo-z galaxies at  $z \sim 2-3$  with  $K_s < 23.4$ .

# $2.2. \ Background \ Quasar \ Samples$

We search for the Ly $\alpha$  forest absorptions found in background quasar spectra in the COSMOS/UltraVISTA

field. Our background quasar spectra are primarily taken from the BOSS Data Release 9 (DR9) Lyman-alpha Forest Catalog (Lee et al. 2013, hereafter L13). L13 has reproduced quasar continua by the technique of meanflux regulated principal component analysis (MF-PCA) continuum fitting (Lee et al. 2012). Because L13 does not include all quasars identified by the SDSS-III surveys (Eisenstein et al. 2011), our background quasar spectra are also taken from the BOSS Data Release 12 (BOSS DR12) and the SDSS-III Data Release 12 (SDSS DR12) (Alam et al. 2015). The BOSS DR9 and DR12 spectra are covered in the wavelength range of 3600-10400Å. The SDSS DR12 spectra are obtained in the wavelength range of 3800-9200Å that is slightly narrower than the BOSS wavelength range. Both the BOSS and the SDSS spectra have the spectral resolution of  $R \equiv \lambda/\Delta\lambda \approx 2000$ .

Because L13 compile spectra of quasars with a redshift range of  $z_{\rm q}>2.15$ , we search for background quasars at  $z_{\rm q}>2.15$  from the BOSS and the SDSS data. We find a total of 26 background quasars in the COSMOS/UltraVISTA field. We remove 4 background quasars that are located at the edge of the COSMOS/UltraVISTA field.

We define the Ly\$\alpha\$ forest wavelength range as 1041 – 1185Å in the quasar rest frame to avoid the Ly\$\beta\$ forest contamination and the proximity effect. In the observed spectra, the Ly\$\alpha\$ forest wavelength range shifts by a factor of  $(1+z_q)$ . We search for background quasars whose Ly\$\alpha\$ forest wavelength ranges cover Ly\$\alpha\$ absorption lines. Because we investigate Ly\$\alpha\$ absorption lines at  $2 \le z_{\text{Ly}\alpha} \le 3$  of the COSMOS/UltraVISTA field, Ly\$\alpha\$ absorption wavelength range is 3647Å  $\le \lambda_{\text{Ly}\alpha}(1+z_{\text{Ly}\alpha}) \le 4862$ Å in the observed frame that requires  $2.08 \le z_q \le 3.67$ . Limiting  $z_q > 2.15$  given by the L13 spectra, we select 21 background quasars at  $2.15 < z_q \le 3.67$ .

Then, we investigate qualities of background quasar spectra. We remove 7 background quasar spectra with  $S/N_{Ly\alpha} < 2$  where  $S/N_{Ly\alpha}$  is the median signal-to-noise ratio (S/N) per pixel over the Ly $\alpha$  forest wavelength range. After the  $S/N_{Ly\alpha} < 2$  cut, we discard 4 broad absorption line (BAL) quasar spectra referring to the SDSS database. In addition, we check background quasar spectra by visual inspection, and remove 1 spectra with large flux fluctuations originated from unknown systematics.

Finally, we use 9 background quasar spectra in the COSMOS/UltraVISTA field. Figure 1 shows the distribution of the background quasars in the COSMOS/UltraVISTA field.

## 3. GALAXY OVERDENSITY AND HI ABSORPTION

#### 3.1. Galaxy Overdensity

We estimate galaxy overdensities around the quasar sightlines where the Ly $\alpha$  forest absorptions are observed. The galaxy overdensities are calculated with the COS-MOS/UltraVISTA catalog (§ 2.1). The galaxy overdensity  $\delta_{\rm gal}$  is defined as

$$\delta_{\rm gal} \equiv \frac{n_{\rm gal}(z)}{\overline{n}_{\rm gal}(z)} - 1,\tag{1}$$

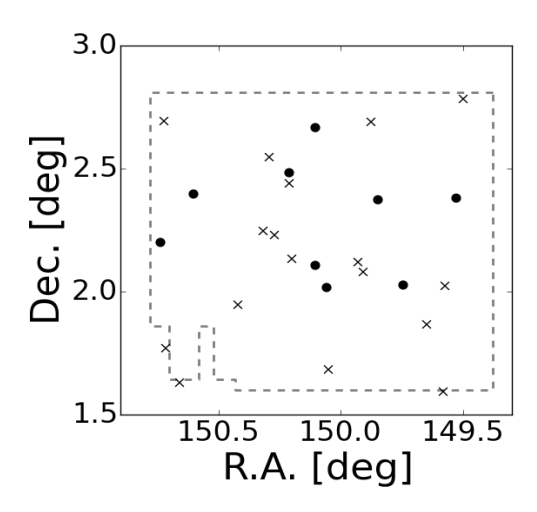


Figure 1. The sky distribution of 26 background quasars found in the COSMOS/UltraVISTA field. Circles and crosses indicate background quasars at z>2.15 used and not used in our analysis, respectively. The grey dashed lines show the area of the COSMOS/UltraVISTA.

where  $n_{\rm gal}$  ( $\overline{n}_{\rm gal}$ ) is the galaxy (average) number density in a cylinder at the redshift z of the cylinder center. The redshift range of  $n_{\rm gal}$  and  $\overline{n}_{\rm gal}$  are defined by the redshift range of the cylinder length. The base area of the cylinder is defined by a radius of r=5' corresponding to an impact parameter of  $\sim 2.5$  pMpc at  $z\sim 2.5$ . The height of the cylinder along a line of sight is given by an average photometric redshift uncertainty. The estimated average photometric redshift uncertainty is  $\sigma_z=0.025(1+z)$  for galaxies with  $K_s<23.4$  mag at  $2\leq z\leq 3$  (Scoville et al. 2013). The error of  $\delta_{\rm gal}$  is estimated with the combination of the photo-z uncertainties and the Poisson errors.

#### 3.2. Ly $\alpha$ forest absorptions

To investigate the Ly $\alpha$  forest absorptions, we do not use spectra in the wavelength range where damped Ly $\alpha$  systems (DLAs) contaminate the spectra. Our spectra consist of spectra taken from the three data sets of L13, the BOSS DR12, and the SDSS DR12 (§ 2.2). The study of L13 has already identified DLAs with the Noterdaeme et al. (2012) catalog, and removed the DLAs from the L13 data sets. We search for DLAs in our BOSS DR12 spectra, referring the Noterdaeme et al. (2012) catalog. We find no DLAs in the Ly $\alpha$  forest wavelength range of our BOSS DR12 spectra. We search DLAs in our SDSS DR12 spectrum by visual inspection, but find no DLAs.

Quasar host galaxies cause intrinsic strong metal absorption lines of SIV  $\lambda 1062.7$ , CIII  $\lambda 1175.7$ , NII  $\lambda 1084.0$ , and NI  $\lambda 1134.4$  in the Ly $\alpha$  forest wavelength range. We mask out the sufficient wavelength width  $\pm$  5Å around these metal absorption lines.

The study of L13 has reproduced quasar continua by the MF-PCA continuum fitting technique (Lee et al. 2012). The MF-PCA continuum fitting technique is essentially composed of two steps: (i) an initial PCA fit to the redward of the Ly $\alpha$  emission line to reproduce the Ly $\alpha$  forest continuum, and (ii) tuning the Ly $\alpha$  forest continuum amplitude extrapolated to the blueward of the Ly $\alpha$  emission line with the cosmic Ly $\alpha$  forest mean transmission of Faucher-Giguère et al. (2008). We obtain

quasar continua of the BOSS DR12 and the SDSS DR12 spectra by the MF-PCA technique in the same manner as L13. We include estimated median r.m.s, continuum fitting errors that are (7, 5.5, 4.5, 4%) for spectra with  $S/N_{Ly\alpha} = (2-4, 4-6, 6-10, 10-15)$  at  $z \sim 2.5-3$  (Lee et al. 2012). We calculate the Ly $\alpha$  forest transmission F(z) at each pixel:

$$F(z) = f(z)/C(z), (2)$$

where f(z) and C(z) are the observed flux and the quasar continuum in the Ly $\alpha$  forest wavelength range, respectively.

We investigate the Ly $\alpha$  forest absorptions in the cylinders used by the galaxy overdensity calculation (§ 3.1). We carry out binning for our spectra with the redshift range of dz = 0.025(1+z) that corresponds to the height of the cylinder, and obtain an average Ly $\alpha$  forest transmission  $\langle F \rangle_{dz}$  and its error  $\langle \sigma_F \rangle_{dz}$ . Here,  $\langle \sigma_F \rangle_{dz}$  is estimated with pixel noises in the spectra and continuum fitting errors. The absorption of the Ly $\alpha$  forest is defined as  $DA \equiv 1 - \langle F \rangle_{dz}$ . We refer to the signal-to-noise ratio of the DA detection  $S/N_{\langle F \rangle}$  as  $DA/\langle \sigma_F \rangle_{dz}$ . We calculate the  $S/N_{\langle F \rangle}$  in the Ly $\alpha$  forest wavelength range, and determine  $z_h$  where  $z_h$  is the redshift of the highest  $S/N_{\langle F \rangle}$ . We put the first cylinder centered at  $z_h$  in each spectrum. We place additional cylinders that lie next to each other around the first cylinder. We use the data of the cylinders with  $S/N_{\langle F \rangle} \geq 4$ , and estimate both  $\delta_{gal}$  and  $\langle F \rangle_{dz}$ in the cylinders. In each cylinder, we calculate the Ly $\alpha$ forest fluctuation whose negative values correspond to a strong Ly $\alpha$  absorption:

$$\delta_{\langle F \rangle} \equiv \frac{\langle F \rangle_{dz}}{F_{\cos}(z)} - 1,\tag{3}$$

where  $F_{\cos}(z)$  is the cosmic Ly $\alpha$  forest mean transmission. We adopt  $F_{\cos}(z)$  estimated by Faucher-Giguère et al. (2008),

$$F_{\cos}(z) = \exp[-0.001845(1+z)^{3.924}]. \tag{4}$$

The error of  $\delta_{\langle F \rangle}$  is estimated with the Ly $\alpha$  forest transmission errors  $\langle \sigma_F \rangle_{dz}$ .

## 4. GALAXY-IGM HI CORRELATION

Figure 2 presents  $\delta_{\rm gal}$  and  $\delta_{\langle F \rangle}$  values in the cylinders. We fit a linear function to the relation of  $\delta_{\rm gal}$ - $\delta_{\langle F \rangle}$ , and obtain the best-fit linear function,

$$\delta_{\langle F \rangle} = -0.17^{+0.06}_{-0.06} - 0.14^{+0.06}_{-0.16} \times \delta_{\text{gal}}$$
 (5)

that is shown with the solid line in Figure 2. Figure 2 and Equation (5) suggest an anti-correlation between  $\delta_{\rm gal}$  and  $\delta_{\langle F \rangle}$ . We calculate Spearman's rank correlation coefficients  $\rho_{\rm obs}$  to investigate the strength of the correlation between  $\delta_{\rm gal}$  and  $\delta_{\langle F \rangle}$ . We obtain  $\rho_{\rm obs} = -0.39$  that corresponds to a  $\sim 90\%$  confidence level. We carry out a bootstrap analysis, and obtain the error of  $\rho_{\rm obs}$  is 0.2 for the 68%-tile interval. This  $\rho_{\rm obs}$  range corresponds to the error of 10% for the 90% confidence level. The anti-correlation between  $\delta_{\rm gal}$  and  $\delta_{\langle F \rangle}$  indicates that high-z galaxies exist around an excess of HI gas in the Lv $\alpha$  forest.

Strong Ly $\alpha$  absorptions can be made by the CGM of galaxies that lie near the quasar sightlines. Rudie et al.

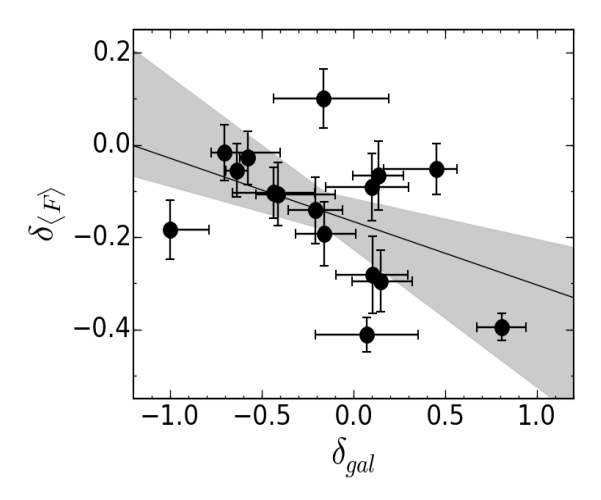


Figure 2. The relation between the galaxy overdensity  $\delta_{\rm gal}$  and the Ly $\alpha$  forest fluctuation  $\delta_{\langle F \rangle}$ . The black circles with error bars represent the galaxy-HI properties of the cylinders. The black solid line shows the best-fit linear function (Equation (5)). The grey shaded area indicates the 68%-tile uncertainty calculated via the bootstrap analysis.

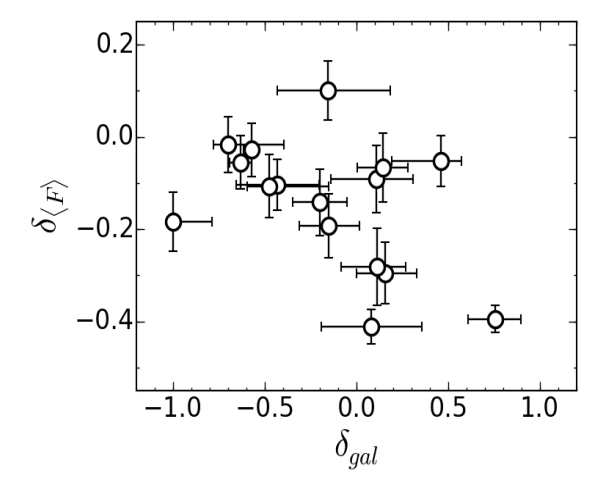


Figure 3. Same as Figure 2, but for revised  $\delta_{\rm gal}$  values whose galaxy numbers are estimated in hollow cylinders whose inner and outer radius is 0.'4 and 5', respectively. An impact parameter of 0.'4 corresponds to that of 200 kpc at  $z\sim2.5$ .

(2012) have studied velocities and spatial locations of HI gas surrounding star-forming galaxies at  $z \sim 2-3$ , and found that the HI column density rapidly increases with decreasing an impact parameter within 200 pkpc. We investigate the Ly $\alpha$  absorptions associated with the CGM. In each cylinder used in § 3.2, we calculate revised  $\delta_{\rm gal}$  values whose galaxy numbers are estimated in hollow cylinders whose inner radius is 0.'4 corresponding to an impact parameter of 200 pkpc. We find that there are only 0-1 galaxies in a 0.4 radius cylinder. The white circles in Figure 3 represent the hollow cylinder results that are very similar to the black circles in Figure 2. Figure 3 indicates no significant differences in the  $\delta_{\rm gal}$ - $\delta_{\langle F \rangle}$  distributions and the  $\rho_{\rm obs}$  value, and suggests that the CGM of galaxies is not the major source of the small  $\delta_{\langle F \rangle}$  values.

#### 5. SIMULATIONS

We perform cosmological hydrodynamical simulations with the RAMSES code (Teyssier 2002) to investigate the spatial correlations of galaxies and IGM HI of our observational results (Section 4). The initial conditions are generated with the COSMIC package (Bertschinger 1995), and are evolved using Zel'dovich approximation. We include both dark matter and baryon using N-body plus Eulerian hydrodynamics on a uniform grid. The simulations are performed in a box size of  $80h^{-1}$  cMpc length with  $512^3$  cells and a spatial resolution of  $156h^{-1}$  ckpc. We use  $512^3$  dark matter particles with a mass resolution of  $3.16 \times 10^8 M_{\odot}$ . The mean gas mass per cell is  $5.4 \times 10^7 M_{\odot}$ .

We include the ultraviolet background model of Haardt & Madau (1996) at the reionization redshift  $z_{\rm reion}=8.5$ , and assume the photoionization equilibrium. We apply the optically thin limit, and do not produce any DLAs.

Dark matter haloes in the simulations are identified with the HOP algorithm (Eisenstein & Hut 1998). We have compared the halo mass functions at  $z \sim 2.5$  in our simulations with the halo mass function of the high resolution N-body simulations (Reed et al. 2007), and found a good agreement. Our simulations resolve dark matter haloes with a mass of  $\log_{10} M_h/M_{\odot} > 11$ .

## 5.1. Mock Galaxy Catalog

We create mock galaxy catalogs from the simulations using the abundance matching technique (e.g., Peacock & Smith 2000; Vale & Ostriker 2004; Moster et al. 2010; Behroozi et al. 2013). We make simulated galaxies, populating each halo with one galaxy. We assume the stellar-to-halo mass ratio (SHMR) with a functional form

$$M_*/M_h = f_0 \frac{(M_h/M_1)^{\alpha}}{1 + (M_h/M_1)^{\alpha-\beta}},$$
 (6)

where  $f_0$ ,  $M_1$ ,  $\alpha$ , and  $\beta$  are free parameters. We produce SMFs at  $z\sim 2.5$  with many sets of these parameters. We compare these SMFs with observed SMFs (Muzzin et al. 2013b; Tomczak et al. 2014), and find the best-fit parameter set reproducing the observed SMFs. With the best-fit parameters, we obtain the SHMR consistent with the SHMR estimated by the abundance matching (Behroozi et al. 2013). We use the simulated galaxies whose stellar mass is  $\log_{10}(M_*/M_\odot) > 9.7$  that is the same stellar mass limit in the COSMOS/UltraVISTA catalog (§2.1). The stellar mass limit corresponds to the minimum halo mass of  $M_h > 4.4 \times 10^{11} M_\odot$ . The simulated galaxies consist of 2221 galaxies at z=2.4-2.5 that agree with the number of galaxies at z=2.4-2.5 in our COSMOS/UltraVISTA photometric samples.

# 5.2. $Ly\alpha$ Forest Catalog

We make mock spectra along the random sightlines parallel to the redshift direction through the simulation box. The Ly $\alpha$  transmitted flux is computed with the fluctuating Gunn-Peterson approximation (e.g., Weinberg et al. 1998, 2003; Meiksin 2009; Becker et al. 2015), that gives the Ly $\alpha$  optical depth as

$$\tau = \frac{c\sigma_{\alpha}\bar{n}_{\rm H}(z)}{\nu_{\alpha}H(z)}x_{\rm HI}\Delta_b \propto \Delta_b^{2-0.72(\gamma-1)},\tag{7}$$

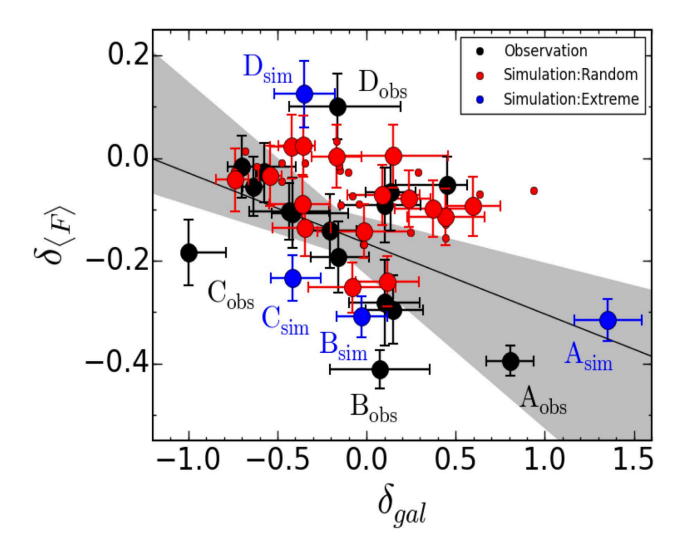


Figure 4. Same as Figure 2, but for the black circles (observation), the red dots (simulations), and the red circles (16 cylinders randomly chosen from the red dots for an example). The blue circles presents cylinders that have extremely large (small) values of  $\delta_{\rm gal}$  and  $\delta_{\langle F \rangle}$  in the simulations (§ 6.2).

where  $\sigma_{\alpha}$  is the Ly $\alpha$  cross section,  $\bar{n}_{\rm H}(z)$  is the cosmic mean density of hydrogen atoms at redshift z,  $\nu_{\alpha}$  is the Ly $\alpha$  resonance frequency, H(z) denotes the Hubble constant at redshift z,  $x_{\rm HI}$  is the fraction of neutral hydrogen,  $\Delta_b$  is the baryonic density in units of the mean density, and  $\gamma$  is the power-law slope of the temperature-density relation in the IGM (Hui & Gnedin 1997). The  $\gamma$  value is set as  $\gamma = 1.5$ that is consistent with observations of the Ly $\alpha$  forest transmissions (Becker et al. 2011; Boera et al. 2014). We investigate the fidelity of our simulated Ly $\alpha$  forest model. We compare the one-dimensional power spectrum of the transmitted flux in our simulations with the SDSS and the BOSS measurements (McDonald et al. 2006; Palanque-Delabrouille et al. 2013), and we find a good agreement. We scale the mean Ly $\alpha$  transmitted flux to the cosmic Ly $\alpha$  forest mean transmission of Faucher-Giguère et al. (2008) (Equation (4)). This scaling method is widely used in the literature (e.g., White et al. 2010; Lukić et al. 2015). We ignore the effect of redshift-space distortion on the Ly $\alpha$  forest. We rebin the simulated spectra, and produce the SDSS and the BOSS pixel width of 69km s<sup>-1</sup>. We add Gaussian noises to the simulated spectra, accomplishing the  $S/N_{Ly\alpha} = 5$ that corresponds to the typical  $S/N_{Ly\alpha}$  in our quasar samples ( $\S 2.2$ ).

# 5.3. Simulated Galaxy-IGM HI Correlation

In Figure 4, the red dots represent a cylinder of  $\delta_{\rm gal}$  and  $\delta_{\langle F \rangle}$  in our simulations. We make 1000 mock catalogs of 16 cylinders that are randomly selected from the simulations, mocking the observational measurements whose number of the cylinders is 16. Similar to the observational results, we fit a linear function to these mock catalogs of 16 cylinders, and identify a weak anti-correlation between  $\delta_{\rm gal}$  and  $\delta_{\langle F \rangle}$  that is one found in our observational results. The red circles in Figure 4 denotes an example mock catalog. We estimate the strength of the anti-correlation with the Spearman's rank correlation coefficients  $\rho_{\rm sim}$  for the 1000 mock catalogs, and find that

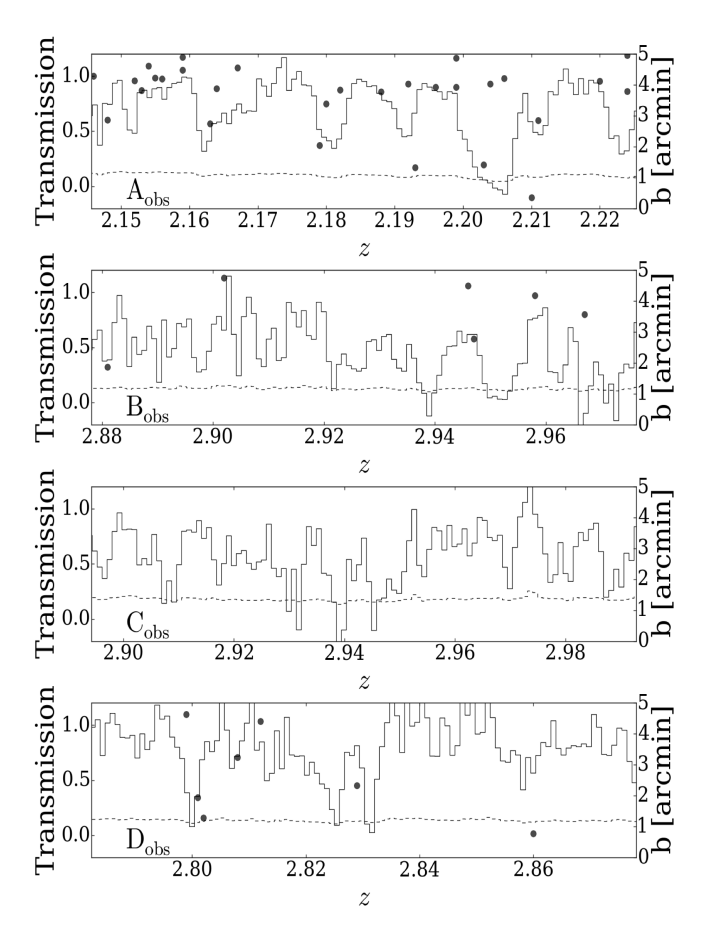


Figure 5. The observed background quasar spectra in the cylinders that have extremely large (small) values of  $\delta_{\rm gal}$  and  $\delta_{\langle F \rangle}$  (§ 6.2). The solid line depicts transmission per pixel as a function of redshift for the Ly $\alpha$  forest absorptions (left-hand axis). The dashed line represents the noise per pixel. The black points denote redshifts and impact parameters (right-hand axis) of our photo-z galaxies in the cylinders. Note that the photometric redshift uncertainty is comparable to the full redshift range of the cylinder.  $\rho_{\rm sim}$  ranges in -0.35-(-0.60) for the 68%-tile interval. This  $\rho_{\rm sim}$  range indicates that our conclusion of  $\sim 90\%$  confidence level can be changed up to 10%.

#### 6. DISCUSSION

# ${\it 6.1. Comparison between the Observation and the } \\ Simulation Results$

Sections 4 and 5.3 present the observation and the simulation results. Both observation and simulation results indicate the weak anti-correlation between  $\delta_{\rm gal}$  and  $\delta_{\langle F \rangle}$  (Figure 4). Moreover, the Spearman's rank correlation coefficient  $\rho_{\rm obs} = -0.39$  from the observations (Section 4) falls in the  $\rho_{\rm sim}$  range of -0.35-(-0.60), indicating that simulations well reproduce observational results.

#### 6.2. Four Cylinders with an extreme value

In Figure 4, we find four cylinders with the labels of  $A_{\rm obs}$ ,  $B_{\rm obs}$ ,  $C_{\rm obs}$ , and  $D_{\rm obs}$  that have extremely large (small) values of  $\delta_{\rm gal}$  and  $\delta_{\langle F \rangle}$ . Note that, in Figure 4, three out of these four cylinders,  $B_{\rm obs}$ ,  $C_{\rm obs}$ , and  $D_{\rm obs}$ , show significant departures from the anti-correlation of  $\delta_{\rm gal}$  and  $\delta_{\langle F \rangle}$ , and weaken the anti-correlation signal. If we exclude these three cylinders, we obtain  $\rho_{\rm obs} = -0.57$  that corresponds to a  $\sim 96\%$  confidence level.

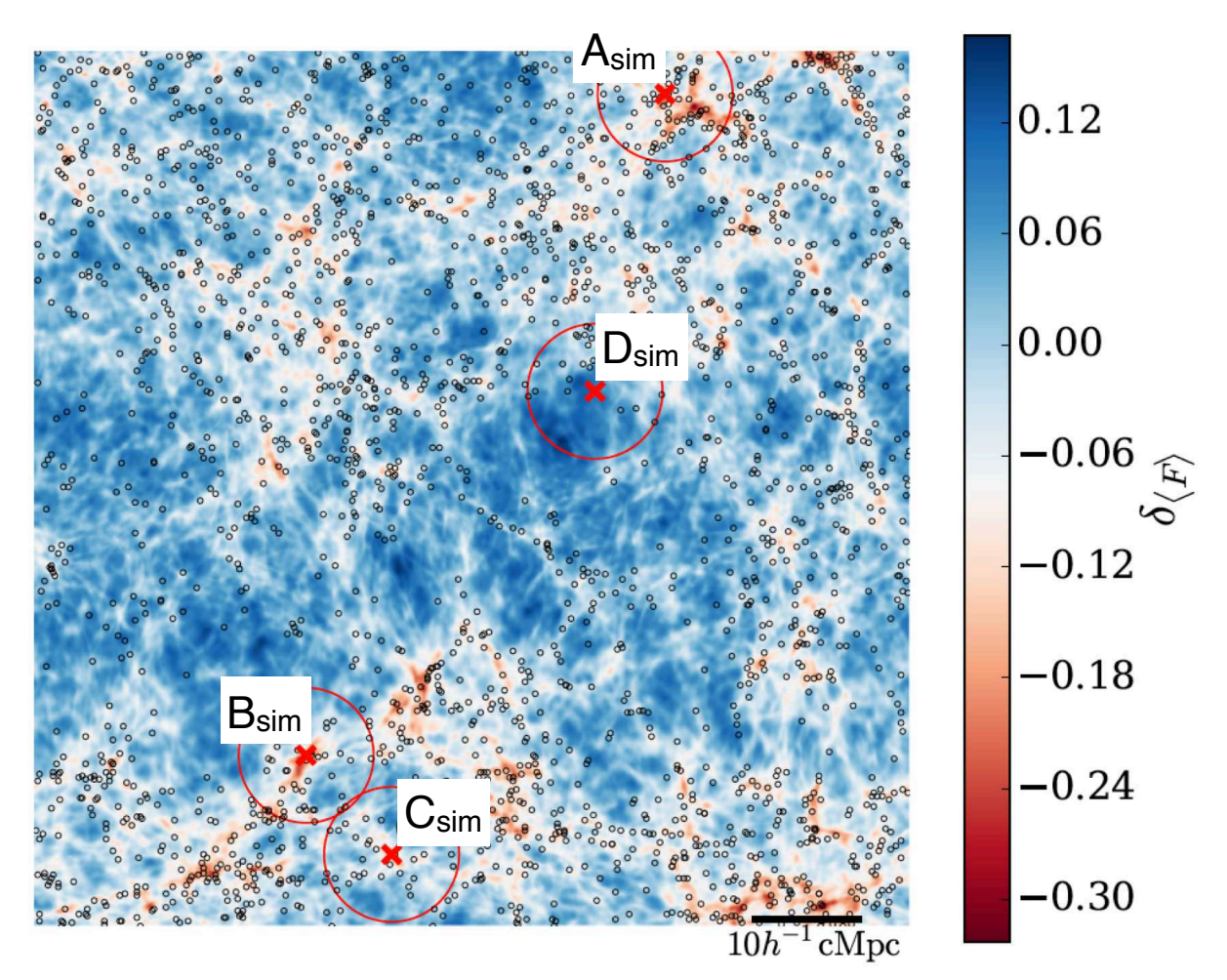


Figure 6. Projected sky map of the distribution of the mock galaxies and the Ly $\alpha$  forest absorptions in the simulations. The  $10h^{-1}{\rm cMpc}$  corresponds to 8.5 at  $z\sim2.5$ . The black circles represents mock galaxies whose stellar mass is  $\log_{10}M_*/M_\odot>9.7$ . Note that the background color represents the projected  $\delta_{\langle F \rangle}$  over the full redshift range ( $\Delta z=0.1$ ) of the simulation box. The positions of sightlines are indicated by the red crosses with red circles showing the radii of the cylinders ( $A_{\rm sim}$ ,  $B_{\rm sim}$ ,  $C_{\rm sim}$ ,  $D_{\rm sim}$ ).

We present background quasar spectra of the four cylinders in Figure 5. The full width of the abscissa axis in the four panels of Figure 5 corresponds to the full redshift range of the cylinder. The black points in Figure 5 present the positions of galaxies with the best estimate of photometric redshifts and the impact parameter b in reference to quasar sightlines. We note that the photometric redshift uncertainty is comparable to the full redshift range of the cylinder.

We investigate the physical origin of the large or the small  $\delta_{\rm gal}$  ( $\delta_{\langle F \rangle}$ ) values in the four cylinders from our observations. We use the simulations performed in Section 5, and search for cylinders in the simulations whose  $\delta_{\rm gal}$ - $\delta_{\langle F \rangle}$  values are similar to the four cylinders from our observations. With the simulation data, we create the sky map (Figure 6), and identify four mock cylinders that show  $\delta_{\rm gal}$ - $\delta_{\langle F \rangle}$  values most similar to  $A_{\rm obs}$ - $D_{\rm obs}$ . We refer to these mock cylinders as the  $A_{\rm sim}$ ,  $B_{\rm sim}$ ,  $C_{\rm sim}$ , and  $D_{\rm sim}$ . The sightline maps and spectra of  $A_{\rm sim}$ - $D_{\rm sim}$  are shown in Figures 7 and 8, respectively. In Figure 4, we overplot the  $\delta_{\rm gal}$ - $\delta_{\langle F \rangle}$  values of  $A_{\rm sim}$ - $D_{\rm sim}$ . Below, we describe properties and comparisons of  $A_{\rm obs}$ - $D_{\rm obs}$  and  $A_{\rm sim}$ - $D_{\rm sim}$ .

Cylinder A:  $A_{obs}$  has the largest  $\delta_{gal}$  and one of the

smallest  $\delta_{\langle F \rangle}$  values. The top panel of Figure 5 indicates that  $A_{\rm obs}$  has the largest number of galaxies and one of the strongest Ly\$\alpha\$ forest absorptions among the four cylinders of  $A_{\rm obs}$ -Dobs. Interestingly,  $A_{\rm obs}$  coincides with one of the proto-cluster candidates reported by Chiang et al. (2014). The large  $\delta_{\rm gal}$  and the small  $\delta_{\langle F \rangle}$  values of  $A_{\rm obs}$  suggest that a large galaxy overdensity is associated with the large amount of HI gas (Cucciati et al. 2014; Chiang et al. 2015; Cai et al. 2015; Lee et al. 2016). Our simulation results in Figure 7 present that the sightline of  $A_{\rm sim}$  penetrates gas filaments of LSSs and a galaxy overdensity like a proto-cluster at  $x \sim 40-50h^{-1}{\rm cMpc}$ . Moreover, the top panel of Figure 8 indicates that  $A_{\rm sim}$  would include a Coherently Strong Ly\$\alpha\$ Absorption system (CoSLA) that traces massive overdensities on the scale of  $\sim 15h^{-1}{\rm cMpc}$  (Cai et al. 2015)

Cylinder B:  $B_{\rm obs}$  has the moderate  $\delta_{\rm gal}$  and the smallest  $\delta_{\langle F \rangle}$  values. The second top panel of Figure 5 shows that  $B_{\rm obs}$  has the strong Ly $\alpha$  forest absorptions over the entire redshift range of the cylinder. In our simulations, Figure 7 presents that the sightline of  $B_{\rm sim}$  goes through gas filaments at  $x \sim 10-30h^{-1}$  cMpc. Our simulations indicate that the sightline of  $B_{\rm obs}$  would penetrate gas

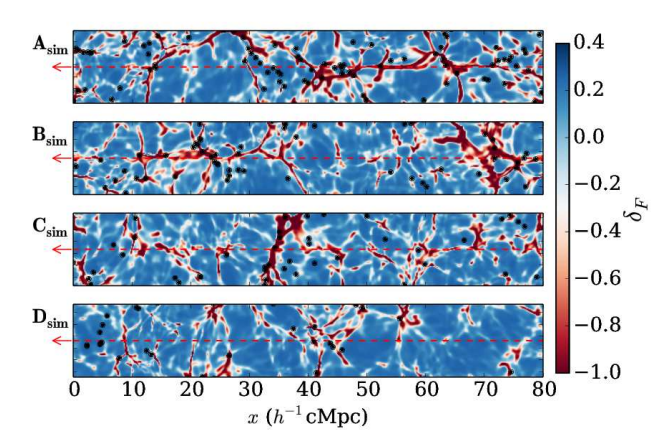


Figure 7. Sightline map of the distribution of the mock galaxies and the Ly $\alpha$  forest absorptions. The red dashed lines represent the sightlines of  $A_{\rm sim}$ ,  $B_{\rm sim}$ ,  $C_{\rm sim}$ , and  $D_{\rm sim}$  (§ 6.2). Note that the panel width corresponds to the  $80h^{-1}$  cMpc length of a box size. The black points are the projected positions of mock galaxies in the cylinders. The background color represents the  $\delta_{\langle F \rangle}$  value per cell on the sightline plane.

filaments with the moderate number of galaxies.

Cylinder C:  $C_{obs}$  has the smallest  $\delta_{gal}$ . Note that  $C_{\rm obs}$  has  $\delta_{\rm gal}=-1$  corresponding to no galaxy in the cylinder. The second bottom panel of Figure 5 indicates that Cobs does not have galaxies but the moderately strong Ly $\alpha$  forest absorptions. In our simulations, we identify  $C_{\text{sim}}$  that has  $\delta_{\text{gal}}$ - $\delta_{\langle F \rangle}$  values most similar to those of Cobs. Our simulation results in Figure 7 shows that the sightline of  $C_{sim}$  penetrates a large void of LSSs at  $x \sim 20h^{-1}$ cMpc and goes across gas filaments at  $x \sim 35 h^{-1} {\rm cMpc}$  region. Our simulations suggest that C<sub>obs</sub> would penetrate a large void, and go across gas filaments. Note that  $C_{\rm sim}$  has  $\delta_{\rm gal} \sim -0.5$  that is larger than the  $\delta_{\rm gal}$  value of  $C_{\rm obs}$ . Our simulations find no cylinders with  $\delta_{\rm gal} = -1$  and  $\delta_{\langle F \rangle} \sim -0.2$ . This is the difference between C<sub>obs</sub> and C<sub>sim</sub>. This is probably because (1) photometric redshifts are catastrophically determined in the  $C_{obs}$ , or (2) the sightline of  $C_{obs}$  penetrates faint galaxies with  $K_s > 23.4$  mag.

Cylinder D: The cylinder with the largest  $\delta_{\langle F \rangle}$  is  $D_{obs}$ . The bottom panel of Figure 5 presents that  $D_{obs}$  has the moderately weak Ly $\alpha$  forest absorptions. In our simulations, Figure 7 shows that the sightline of  $D_{sim}$  crosses the low-density filaments. Our simulation results suggest that  $D_{obs}$  would go through the orthogonal low-density filaments.

#### 6.3. Summary of the simulation comparisons

In  $\S$  6.2, we discuss the physical origins of four cylinders  $(A_{\rm obs}, B_{\rm obs}, C_{\rm obs}, D_{\rm obs})$  that have extremely large (small) values of  $\delta_{\rm gal}$  and  $\delta_{\langle F \rangle}$ . We use the simulations performed in Section 5, and identify four cylinders  $(A_{\rm sim}, B_{\rm sim}, C_{\rm sim}, D_{\rm sim})$  whose  $\delta_{\rm gal}$ - $\delta_{\langle F \rangle}$  values are close to  $(A_{\rm obs}, B_{\rm obs}, C_{\rm obs}, D_{\rm obs})$ . The comparisons between  $A_{\rm obs}$ - $D_{\rm obs}$  and  $A_{\rm sim}$ - $D_{\rm sim}$  suggest that sightlines in the observation would penetrate (1) a galaxy overdensity like a protocluster in  $A_{\rm obs}$ , (2) gas filaments in  $B_{\rm obs}$ , (3) a large void in  $C_{\rm obs}$ , and (4) orthogonal low-density filaments in  $D_{\rm obs}$ . In this way, our simulations provide the possible physical pictures of these four cylinders based on the structure formation models.

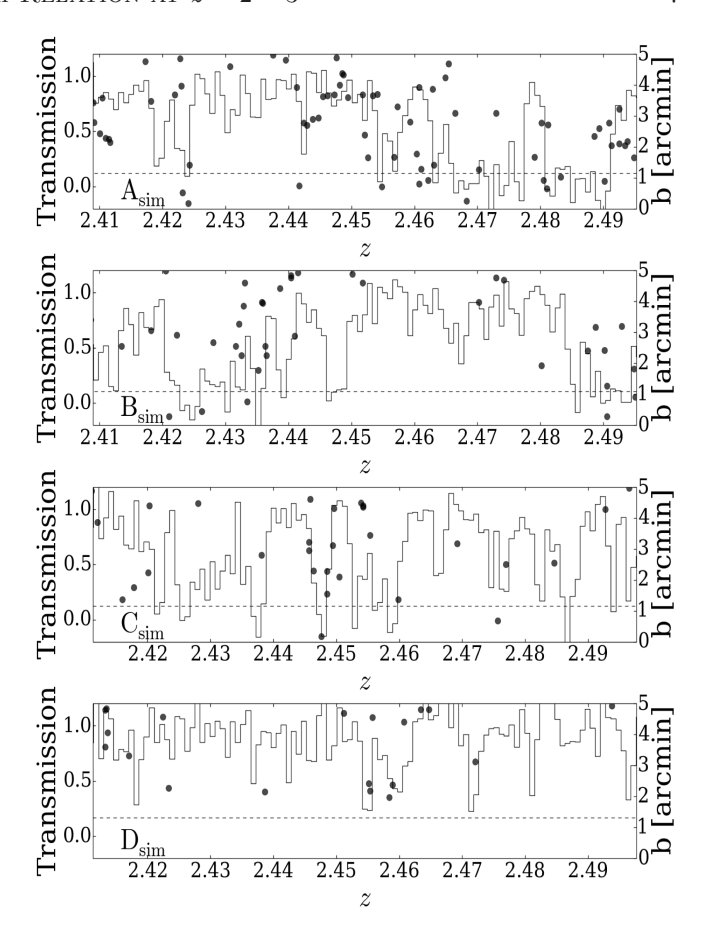


**Figure 8.** Same as Figure 5, but for the background quasar spectra in the cylinders that have extremely large (small) values of  $\delta_{\rm gal}$  and  $\delta_{\langle F \rangle}$  in the simulations (§ 6.2).

The similarity between our observation and simulation results (Figure 4) supports the standard picture of galaxy formation scenario in the filamentary LSSs (Mo et al. 2010) on which our simulations are based.

As noted in Section 6.2, the three cylinders,  $B_{\rm obs}$ ,  $C_{\rm obs}$ , and  $D_{\rm obs}$  depart from the anti-correlation of  $\delta_{\rm gal}$  and  $\delta_{\langle F \rangle}$  in Figure 4. Because the simulation counterparts of these three cylinders penetrate gas filaments, a large void, and orthogonal low-density filaments by chance, the comparisons with our simulations suggest that the significant departures from the anti-correlation are produced by the filamentary LSSs and the observation sightlines. These chance alignment effects reduce the anti-correlation signal.

# 7. SUMMARY

We investigate spatial correlations of galaxies and IGM HI with the 13,415 photo-z galaxies and the Ly $\alpha$  forest absorptions of the background quasars with no signature of damped Ly $\alpha$  system contamination in the 1.62 deg<sup>2</sup> COSMOS/UltraVISTA field. The results of our study are summarized below.

1. We estimate the Ly $\alpha$  forest fluctuation  $\delta_{\langle F \rangle}$  and the galaxy overdensity  $\delta_{\rm gal}$  within the impact parameter of 2.5 pMpc from the quasar sightlines at  $z \sim 2-3$ . We identify an anti-correlation between  $\delta_{\rm gal}$  and  $\delta_{\langle F \rangle}$  values (Figure 2). The Spearman's  $\rho$ 

value of -0.39 indicates that there is a weak anticorrelation between  $\delta_{\rm gal}$  and  $\delta_{\langle F \rangle}$  at a  $\sim 90\%$  confidence level. This anti-correlation suggests that high-z galaxies are found in the excess regions of H<sub>I</sub> gas in the Ly $\alpha$  forest.

- 2. We perform cosmological hydrodynamical simulations with the RAMSES code, and identify an anti-correlation between  $\delta_{\rm gal}$  and  $\delta_{\langle F \rangle}$  values in our simulation model that is similar to the one found in our observational data. We estimate the Spearman's  $\rho$  for the  $\delta_{\rm gal}$  and  $\delta_{\langle F \rangle}$  values in our simulation results that suggest the anti-correlation agreeing with the observational results.
- 3. In our observational data, we identify four cosmic volumes that have very large or small values of  $\delta_{\rm gal}$  and  $\delta_{\langle F \rangle}$  that are dubbed  $A_{\rm obs}$ ,  $B_{\rm obs}$ ,  $C_{\rm obs}$ , and  $D_{\rm obs}$  (Figure 4). Three out of these four cylinders,  $B_{\rm obs}$ ,  $C_{\rm obs}$ , and  $D_{\rm obs}$ , present significant departures from the anti-correlation of  $\delta_{\rm gal}$  and  $\delta_{\langle F \rangle}$ , and weaken the signal of the anti-correlation.
- 4. In our simulations, we identify model counterparts of  $A_{\rm obs}$ ,  $B_{\rm obs}$ ,  $C_{\rm obs}$ , and  $D_{\rm obs}$  in the  $\delta_{\rm gal}$  and  $\delta_{\langle F \rangle}$  plane (Figure 4), which are referred to as  $A_{\rm sim}$ ,  $B_{\rm sim}$ ,  $C_{\rm sim}$ , and  $D_{\rm sim}$ , respectively. The comparisons of  $A_{\rm obs}$ - $D_{\rm obs}$  with  $A_{\rm sim}$ - $D_{\rm sim}$  indicate that the observations pinpoint (1) a galaxy overdensity like a proto-cluster in  $A_{\rm obs}$ , (2) gas filaments lying on the quasar sightline by chance in  $B_{\rm obs}$ , (3) a large void in  $C_{\rm obs}$ , and (4) orthogonal low-density filaments in  $D_{\rm obs}$ . Our simulations suggest that the three cylinders,  $B_{\rm obs}$ ,  $C_{\rm obs}$ , and  $D_{\rm obs}$  significantly departing from the anti-correlation are produced by the filamentary LSSs and the observation sightlines. The chance alignment effects reduce the anti-correlation signal of  $\delta_{\rm gal}$  and  $\delta_{\langle F \rangle}$ .

The large-scale correlation of  $\delta_{\mathrm{gal}}$ - $\delta_{\langle F \rangle}$  found in Section 4 is relatively weak. This is because the correlation is based on the relatively large cylinder whose redshift range is limited in photo-z accuracy (see Figure 1 of Cai et al. 2015). The small-scale galaxy-H<sub>I</sub> relations can be studied with galaxies with spectroscopic redshifts. Here, the Hobby-Eberly Telescope Dark Energy Experiment (HETDEX) survey (Hill et al. 2004) will carry out the wide-field observations, and provide 0.8 million galaxies in  $\sim 400 \text{ deg}^2$ . The HETDEX survey will reveal the galaxy-HI relations in the large cosmological volumes including a number of proto-cluster cadidates, gas filaments, and voids of LSSs. The galaxy-IGM relation study with HETDEX will be complementary to the programs of the MAMMOTH (Cai et al. 2015) and the CLAMATO (Lee et al. 2014, 2016).

We are grateful to Toru Misawa, Suzuka Koyamada, Toru Yamada, Ken Mawatari, Takashi Kojima, and Andreas Schulze for their useful comments and constructive discussions. We are also grateful to Khee-Gan Lee for kindly providing the MF-PCA code.

The COSMOS/UltraVISTA  $K_s$ -band selected galaxy catalog used in this work is compiled by Muzzin et al.

(2013a). The catalog contains PSF-matched photometry in 30 photometric bands covering the wavelength range  $0.15\mu\mathrm{m} \rightarrow 24\mu\mathrm{m}$  and includes the available GALEX (Martin et al. 2005), CFHT/Subaru (Capak et al. 2007), UltraVISTA (McCracken et al. 2012), S-COSMOS (Sanders et al. 2007), and zCOSMOS (Lilly et al. 2009) datasets.

Funding for SDSS-III has been provided by the Alfred P. Sloan Foundation, the Participating Institutions, the National Science Foundation, and the U.S. Department of Energy Office of Science. The SDSS-III Web site is http://www.sdss3.org/. SDSS-III is managed by the Astrophysical Research Consortium for the Participating Institutions of the SDSS-III Collaboration including the University of Arizona, the Brazilian Participation Group, Brookhaven National Laboratory, University of Cambridge, Carnegie Mellon University, University of Florida, the French Participation Group, the German Participation Group, Harvard University, the Instituto de Astrofisica de Canarias, the Michigan State/Notre Dame/JINA Participation Group, Johns Hopkins University, Lawrence Berkeley National Laboratory, Max Planck Institute for Astrophysics, Max Planck Institute for Extraterrestrial Physics, NewMexico State University, New York University, Ohio State University, Pennsylvania State University, University of Portsmouth, Princeton University, the Spanish Participation Group, University of Tokyo, University of Utah, Vanderbilt University, University of Virginia, University of Washington, and Yale University.

This work is supported by World Premier International Research Center Initiative (WPI Initiative), MEXT, Japan, and KAKENHI (15H02064) Grant-in-Aid for Scientific Research (A) through Japan Society for the Promotion of Science (JSPS).

### REFERENCES

Adelberger, K. L., Shapley, A. E., Steidel, C. C., et al. 2005, ApJ, 629, 636

Adelberger, K. L., Steidel, C. C., Shapley, A. E., & Pettini, M. 2003, ApJ, 584, 45

Alam, S., Albareti, F. D., Allende Prieto, C., et al. 2015, ApJS, 219, 12

Becker, G. D., Bolton, J. S., Haehnelt, M. G., & Sargent, W. L. W. 2011, MNRAS, 410, 1096

Becker, G. D., Bolton, J. S., & Lidz, A. 2015, PASA, 32, e045 Becker, G. D., Hewett, P. C., Worseck, G., & Prochaska, J. X.

2013, MNRAS, 430, 2067 Behroozi, P. S., Wechsler, R. H., & Conroy, C. 2013, ApJ, 770, 57 Bertschinger, E. 1995, ArXiv Astrophysics e-prints, astro-ph/9506070

Boera, E., Murphy, M. T., Becker, G. D., & Bolton, J. S. 2014, MNRAS, 441, 1916

Cai, Z., Fan, X., Peirani, S., et al. 2015, ArXiv e-prints, arXiv:1512.06859

Capak, P., Aussel, H., Ajiki, M., et al. 2007, ApJS, 172, 99 Chiang, Y.-K., Overzier, R., & Gebhardt, K. 2014, ApJ, 782, L3 Chiang, Y.-K., Overzier, R. A., Gebhardt, K., et al. 2015, ApJ,

Crighton, N. H. M., Bielby, R., Shanks, T., et al. 2011, MNRAS, 414, 28

Cucciati, O., Zamorani, G., Lemaux, B. C., et al. 2014, A&A, 570, A16

Eisenstein, D. J., & Hut, P. 1998, ApJ, 498, 137

Eisenstein, D. J., Weinberg, D. H., Agol, E., et al. 2011, AJ, 142, 72

Faucher-Giguère, C.-A., Prochaska, J. X., Lidz, A., Hernquist, L., & Zaldarriaga, M. 2008, ApJ, 681, 831

- Haardt, F., & Madau, P. 1996, ApJ, 461, 20
- Harikane, Y., Ouchi, M., Ono, Y., et al. 2016, ApJ, 821, 123
- Hill, G. J., Gebhardt, K., Komatsu, E., & MacQueen, P. J. 2004,
  in American Institute of Physics Conference Series, Vol. 743,
  The New Cosmology: Conference on Strings and Cosmology,
  ed. R. E. Allen, D. V. Nanopoulos, & C. N. Pope, 224–233
- Hui, L., & Gnedin, N. Y. 1997, MNRAS, 292, 27
- Lee, K.-G., Suzuki, N., & Spergel, D. N. 2012, AJ, 143, 51
- Lee, K.-G., Bailey, S., Bartsch, L. E., et al. 2013, AJ, 145, 69
- Lee, K.-G., Hennawi, J. F., Stark, C., et al. 2014, ApJ, 795, L12 Lee, K.-G., Hennawi, J. F., White, M., et al. 2016, ApJ, 817, 160
- Lee, K.-G., Hennawi, J. F., White, M., et al. 2016, ApJ, 817, 160 Lee, K.-S., Giavalisco, M., Conroy, C., et al. 2009, ApJ, 695, 368
- Lilly, S. J., Le Brun, V., Maier, C., et al. 2009, ApJS, 184, 218 Lukić, Z., Stark, C. W., Nugent, P., et al. 2015, MNRAS, 446,
- 3697 Martin, D. C., Fanson, J., Schiminovich, D., et al. 2005, ApJ, 619, L1
- Mawatari, K., Inoue, A. K., Kousai, K., et al. 2016, ApJ, 817, 161
  McCracken, H. J., Milvang-Jensen, B., Dunlop, J., et al. 2012, A&A, 544, A156
- McDonald, P., Seljak, U., Burles, S., et al. 2006, ApJS, 163, 80 Meiksin, A. A. 2009, Reviews of Modern Physics, 81, 1405
- Mo, H., van den Bosch, F. C., & White, S. 2010, Galaxy
- Formation and Evolution (Cambridge: Cambridge Univ. Press) Moster, B. P., Somerville, R. S., Maulbetsch, C., et al. 2010, ApJ,
- Muzzin, A., Marchesini, D., Stefanon, M., et al. 2013a, ApJS, 206, 8
- —. 2013b, ApJ, 777, 18
- Noterdaeme, P., Petitjean, P., Carithers, W. C., et al. 2012, A&A, 547, L1
- Oke, J. B., & Gunn, J. E. 1983, ApJ, 266, 713
- Palanque-Delabrouille, N., Yèche, C., Borde, A., et al. 2013, A&A, 559, A85
- Peacock, J. A., & Smith, R. E. 2000, MNRAS, 318, 1144

- Planck Collaboration, Ade, P. A. R., Aghanim, N., et al. 2015, ArXiv e-prints, arXiv:1502.01589
- Prochaska, J. X., Hennawi, J. F., Lee, K.-G., et al. 2013, ApJ, 776, 136
- Rakic, O., Schaye, J., Steidel, C. C., & Rudie, G. C. 2012, ApJ, 751, 94
- Reed, D. S., Bower, R., Frenk, C. S., Jenkins, A., & Theuns, T. 2007, in Astronomical Society of the Pacific Conference Series, Vol. 379, Cosmic Frontiers, ed. N. Metcalfe & T. Shanks, 12
- Rudie, G. C., Steidel, C. C., Trainor, R. F., et al. 2012, ApJ, 750,
- Sanders, D. B., Salvato, M., Aussel, H., et al. 2007, ApJS, 172, 86Schechter, P. 1976, ApJ, 203, 297
- Scoville, N., Aussel, H., Brusa, M., et al. 2007, ApJS, 172, 1
- Scoville, N., Arnouts, S., Aussel, H., et al. 2013, ApJS, 206, 3Steidel, C. C., Erb, D. K., Shapley, A. E., et al. 2010, ApJ, 717, 289
- Teyssier, R. 2002, A&A, 385, 337
- Thomas, R., Le Fèvre, O., Cassata, V. L. B. P., et al. 2014, ArXiv e-prints, arXiv:1411.5692
- Tomczak, A. R., Quadri, R. F., Tran, K.-V. H., et al. 2014, ApJ, 783, 85
- Turner, M. L., Schaye, J., Steidel, C. C., Rudie, G. C., & Strom, A. L. 2014, MNRAS, 445, 794
- Vale, A., & Ostriker, J. P. 2004, MNRAS, 353, 189
- Weinberg, D. H., Davé, R., Katz, N., & Kollmeier, J. A. 2003, in American Institute of Physics Conference Series, Vol. 666, The Emergence of Cosmic Structure, ed. S. H. Holt & C. S. Reynolds, 157–169
- Weinberg, D. H., Burles, S., Croft, R. A. C., et al. 1998, ArXiv Astrophysics e-prints, astro-ph/9810142
- White, M., Pope, A., Carlson, J., et al. 2010, ApJ, 713, 383